Burst and collapse in traveling-wave convection of a binary fluid

Eran Kaplan, Eugenii Kuznetsov,* and Victor Steinberg
Department of Nuclear Physics, The Weizmann Institute of Science, Rehovot 76100, Israel
(Received 5 November 1993; revised manuscript received 25 May 1994)

We report experimental results of a traveling-wave burst and collapse process occurring in convecting binary mixtures in a wide range of the control parameters. Analysis in the framework of the one-dimensional complex Ginzburg Landau (CGL) equation reveals an alternative self-focusing mechanism responsible for this behavior: faster than exponential bursting due to the destabilizing effect of the nonlinearity and collapse due to suppression of the pulse growth at the edges, leading to the destruction of the pulse by compression. The latter effect is associated with the strong nonlinear dispersion of the system. Numerical analysis, based on the CGL equation, closely matches both experimental results and theoretical considerations. The limits of validity of the proposed mechanism are also discussed.

PACS number(s): 47.27.Te, 47.20.Ky, 47.52.+j

I. INTRODUCTION

In this paper we report experimental, numerical, and theoretical observations of wave collapse, occurring in one dimensional (1D) traveling wave (TW) convection in binary mixtures. Wave collapse, namely, the formation, in a finite time, of a singularity from an initially uniform amplitude field, has been the subject of intensive studies in recent years [1]. This process, appearing, as an example, in plasma physics, nonlinear optics, and nonlinear surface waves is usually the most effective mechanism of transforming wave energy into heat. Several mechanisms explaining such behavior have been proposed, of which the framework of the nonlinear Schrödinger (NLS) equation is the most advanced [1,2].

In the past few years, Rayleigh-Bénard convection in binary mixtures has been the subject of intense scientific activity. The most important reasons for this interest are the fact that this system undergoes a Hopf bifurcation to a TW state as a first transition, in a wide range of its parameter space [3,4], and the fact that the system exhibits a wealth of fascinating TW patterns near the onset of convection [3,8]. Moreover, the experiments can be performed with excellent accuracy and the underlying equations are well understood [5–7].

A thin, horizontal layer of a binary fluid mixture of height d, heated from below, exhibits convective patterns above a critical temperature difference ΔT_c. There are four control parameters, which completely characterize the transition to a convective state in a horizontally infinite cell. The first parameter is the Rayleigh number R, which is proportional to the temperature difference ΔT applied across the layer. The second parameter is the separation ratio ψ, characterizing the relative importance of the concentration gradient induced by the Soret effect and the temperature gradient. The Prandtl number, $P = \frac{\nu}{\kappa}$, and the Lewis number $L = \frac{D}{\kappa}$ (ν is the kinematic viscosity, D, κ are the mass and thermal diffusivities, respectively), characterize the fluid. In a finite rectangular cell, the reflection coefficient of the TW at the endwalls can be regarded as an effective fifth control parameter [9,10]. If the convection cell is narrow enough, convection patterns may be considered as essentially one dimensional [3], and the nonlinear behavior of the system close to the onset can be described by two coupled 1D complex Ginzburg-Landau (CGL) equations [11,12]:

$$\begin{aligned}\tau_0(\partial_t \pm s\partial_x)A_{r,l} &= \epsilon A_{r,l} + (1+ic_1)\xi_0^2\partial_x^2 A_{r,l} \\ &\quad + g(1+ic_2)|A_{r,l}|^2 A_{r,l} + g_1(1+ic_3)|A_{l,r}|^2 A_{r,l} \ . \end{aligned} \tag{1}$$

Here $A_{r,(l)}$ are the amplitudes of the right (left) TW respectively, $\epsilon = \frac{R-R_c}{R_c}$ is the experimental control parameter (R_c is the convection threshold value of R), s is the group velocity of the TW, τ_0 and ξ_0 are the characteristic time and length, respectively, c_1 is the linear dispersion coefficient, c_2 is the nonlinear dispersion coefficient, and g, g_1, and c_3 are real parameters. All parameters have been calculated as a function of ψ, P, and L [5,6]. In the experiments that we describe, g is positive (destabilizing) and varies in the range between 0.15 and 0.22 [7]. We are interested here in the dynamics of the TW state, characterized by the chaotic repetitive formation and collapse of TW bursts. This state is observed in both long enough rectangular [3,8] and annular [15,16] convection cells, and was called the "chaotic blinking" state [3]. Due to the absence of reflection effects, the appearance of this state is probably more spectacular in annular geometry. In 1983, Bretherton and Spiegel [13] showed that the 1D-CGL equation exhibits such erratic behavior, if, in the limit of $c_2 \gg 1$, one assumes the nonlinear term to be purely imaginary. They showed that an initially growing inhomogeneity in the amplitude field decays due to

*Also at Landau Institute for Theoretical Physics, 2 Kosygin st., Moscow 117334, Russia.

an effective decrease of ϵ, which is induced by the large nonlinear dispersivity of the system. In this limit, the amplitude growth can be described by a linear equation, and the pulse width [defined at full width half maximum (FWHM) of the pulse] is almost constant throughout its growth. Recently, Kolodner *et al.* identified the source of the "blinking" behavior in the strong nonlinear dispersivity of the system [15,16]. They showed that the dynamics *qualitatively* resemble the numerical simulations of Ref. [13], as well as the result of more recent work [14], which scanned the parameter space relevant to convection in binary mixtures. Thus, the state was coined "dispersive chaos" [15].

Here, we present quantitative studies of the burst and collapse mechanism analytically, experimentally, and in numerical simulations. We found that the burst suppression mechanism proposed by Bretherton and Spiegel works only for the narrowest pulses. For initially wider pulses, the bursting mechanism is strongly nonlinear, and exhibits a self-focusing behavior, namely, much steeper amplitude growth, accompanied by rapid narrowing of the pulse before its collapse. The narrowing is completed before the collapse, which occurs due to compression of the pulse from its edges. The alternative approach suggested in this paper provides a quantitative understanding of all the main features of this state [17]. Sections II and III present the experimental system and results, together with numerical simulations that we conducted. Section IV describes the mechanism of bursting and collapse and compares it to the previously suggested one. We conclude the paper with a discussion and conclusions.

II. EXPERIMENTAL PROCEDURE

The experimental apparatus is an improved version of a previously described one [3,8]. The convective layer is sandwiched between a sapphire window and a nickel plated copper mirror on the bottom. The lateral walls of the convection cell are made of polypropylene, having low thermal conductivity ($\lambda = 1.2$ mW/cm K) and low absorption of the fluid. We used cells of height d in the range $d = 0.182$–0.189 cm. The uniformity of the height was adjusted interferometrically to within $1-2$ μm. The cells were of length $l = \Gamma d$, with Γ between 20 and 40.6, and width of $2d$. Cooling water flowing azimuthally across the narrow side of the convection cell regulates the ambient temperature to $\approx 31\,^{\circ}$C. The bottom plate was heated electrically. The typical long term temperature difference across the layer was regulated to within 0.3 mK, allowing a resolution of $\sim 10^{-5}$ in R.

The experimental fluids were ethanol-water mixtures with weight concentrations of 26–28.5 %. For this range of concentrations the values of ψ vary from -0.065 to -0.005, respectively. The Prandtl and Lewis numbers were almost constant at $P \approx 18$ and $L \approx 0.012$.

We visualize the flow using shadowgraph visualization. It can be shown [18] that if the image plane is far away from the optical caustic plane, then the image intensity is linearly proportional to the convection amplitude. By adjusting the position of the image plane, we mapped the height of the caustic plane as a function of the convection amplitude. Thus we were able to work in the linear optical signal regime even for large amplitudes, in spite of the fact that the dynamic range of the convection amplitude in the "bursting TW" state was about 10^4. We measured the optical intensity along the cell length using a CCD camera, with a resolution better than 10 pixels/roll.

Measurements of the optical signal intensity, as well as measurements of ΔT and of q, the heat flux applied across the convection cell, were performed at prefixed time intervals, at least four times per oscillation period. Apart from background subtraction, no other filtering or enhancement technique was applied to the data. We extracted of the left and right TW amplitudes $A_{l,r}(x,t)$ and their phase by performing complex 2D demodulation. The Hilbert transform algorithm described in Sec. V of Ref. [19] has been used.

In order to compare our results with theoretical predictions, we also performed numerical simulations on the CGL equation. The justification for this procedure will be explained in the next section. Implicit, variable time step algorithm, with periodical boundary conditions was used. The coefficient values were taken from Refs. [5] and [6]. As initial conditions we used either a small amplitude, finite width pulse or a small amplitude analytic solution of the NLS equation. The simulations were performed on either the third or fifth order CGL equation, with no significant differences observed. The reason for this will be clarified below.

III. EXPERIMENTAL RESULTS

For the range of parameters relevant to our experiments, the system becomes convectively unstable and undergoes a subcritical Hopf bifurcation to a TW convective state, above a critical temperature difference, ΔT_c. In the immediate vicinity of the onset ($\epsilon \leq 0.03$), a sequence of patterns, very different in character, appears. The first state observed above the onset is the counterpropagating waves state [3]. In this weakly nonlinear state left (right) TW grow as they travel towards the left (right) endwall of the convection cell. Near the middle of the cell, a source of TW is formed, where the amplitudes of the left and the right propagating waves are equal. This state is stable in a narrow range of the control parameter above the onset (typically for $\epsilon \leq 1 \times 10^{-3}$) [3]. For higher values of ϵ (typically up to $\epsilon \approx 0.015$ in our experiments), the left-right symmetry of the pattern is broken, and "blinking" TW state appears. In this state the amplitude of the TW waves becomes spatially and temporally modulated. In short enough rectangular cells, for small values of ϵ and at higher values of $|\psi|$, the behavior is quasiperiodic, and regular " blinking" behavior was observed [3,4]. This behavior was observed also for specific, accurately tuned values of the cell length [4,20,21]. In the case of either longer cells, or larger value of ϵ, or smaller values of $|\psi|$, periodicity is lost, and convection is characterized by repetitive evolution and collapse of TW bursts, which appear at random times and locations in the convection cell [3,8]. This state and its dynamics are the subject of the

present paper. At still higher values of ϵ, a localized TW state appears. In this state, a solitonlike coherent structure occurs: only a small part of the convection cell is convecting, while the rest of the cell is conducting [3,8]. This state loses stability, with increasing ϵ, to the extended TW state, in which the convection TW becomes absolutely unstable, and the convective state is characterized by very low frequency ($\omega/\omega_0 \sim 0.01$), where ω_0 is the TW frequency at the onset of convection [3].

Typical dynamics of the "chaotic" blinking state is shown in Fig. 1, by means of a space-time plot of the convection amplitude in the cell. This kind of behavior is observed in very long cells ($\Gamma > 30$) for all values of $\epsilon > 0$, up to the transition to the localized TW (LTW) state [3]. Figure 2(a) demonstrates the amplitude at one point in the cell as a function of time. Figure 2(b) presents the power spectrum of the same data. The amplitude is highly irregular, with a power spectrum that is essentially flat in a wide band between the neutral frequency ω_0 and the frequency at which LTW appear (at about $\omega_0/2$). This erratic behavior persists for very long periods of time. Our longest run was over two weeks with the same experimental parameters, without noticeable change in the behavior.

There are several factors which contribute to the spatiotemporal dynamics of weakly nonlinear TW. These are selective linear spatial growth, end wall reflection, nonlinear saturation, nonlinear wave interaction and nonlinear dispersion. The relative contribution of each of these factors varies with changing the control parameters ϵ, ψ and the aspect ratio Γ. For convection cells of moderate aspect ratios ($\Gamma \leq 20$), for $\psi < -0.05$ and for values of ϵ well below the transition to the LTW state, the amplitudes of the left- and the right-going waves are usually of the same order of magnitude. In this case, the linear growth, reflection and nonlinear wave interaction dominate the dynamics. Thus, counter propagating waves or regularly modulated TW (coined "blinking" TW) were observed in cells of $\Gamma = 12$, and in the longer cell of $\Gamma = 20$ for $\psi = -0.058, \epsilon \leq 5 \times 10^{-4}$ [3]. As ϵ increases the regular state gives is replaced by the "chaotic blinking" state. This transition was described in detail in Ref. [3].

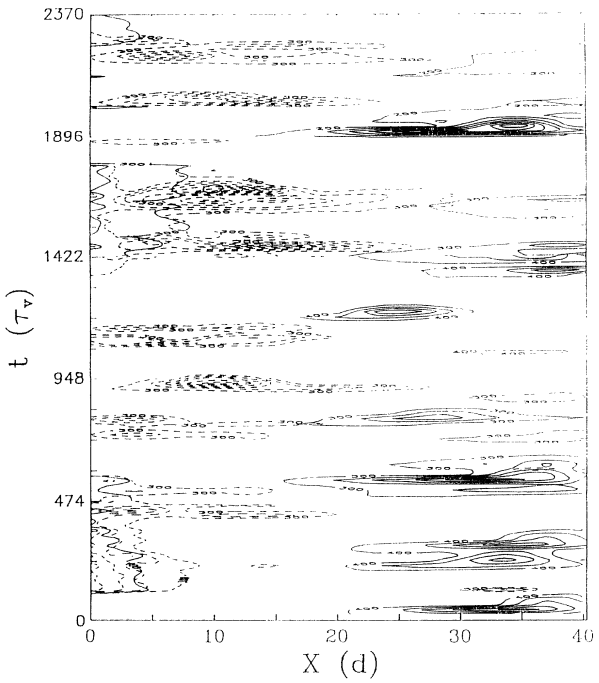

FIG. 1. Spatiotemporal topographical representation of the chaotic "blinking" state. The solid and dashed lines show equal amplitude contours of the right- and left-going TW, respectively. $\psi = -0.032; \epsilon = 0.0094; \Gamma = 40.6$. τ_v, the vertical diffusion time, is equal to 32.3 sec.

In either longer cells, or at $|\psi| < 0.05$, the process of bursting and collapse can be completed, as indeed happens rather often (Fig. 1), before the high amplitude TW packet reaches the lateral wall. Thus, the amplitude near the lateral wall are usually very small, and reflection does not play an important role in the evolution of subsequent pulses. In order to verify this point, we calculated the cross-correlation function between the left and the right TW amplitudes for the cell of $\Gamma = 40.6$ at several values of ϵ. If reflection should play any role in the dynamics of the state, one would expect appearance of a peak in the cross-correlation function at a time delay which is of the order of the cell traversing time. No such behavior was found, pointing out that the bursts appear at random. This result should be compared with Fig. 1(b) of Ref. [3], which shows clear periodic behavior for the regular "blinking" state.

Typically, at the position of a burst, the ratio of the the amplitudes of the left- and right-going waves is $O(100)$. Thus, the role of the nonlinear wave interaction becomes insignificant, can be neglected, and the amplitude equations for the left- and right-propagating waves are uncoupled. Close to the collapse, the convection amplitude is "spiky." The relative amplitude growth rate at the end of bursting, $\frac{1}{A}\frac{\Delta A}{\tau_0}$ exceeds, by at least an order of magnitude, the expected linear amplitude growth rate (e.g., in Figs. 1 and 2). We may safely neglect, in this case, nonlinear saturation, which is expected to produce rounding effects. Thus, only cubic nonlinearity is needed in the amplitude equation which becomes

$$\tau_0 A_t + s A_x = \epsilon A + \xi_0^2 (1 + i c_1) A_{xx} + g(1 + i c_2)|A|^2 A, \tag{2}$$

where A stands for either A_r or A_l. Numerical simulations based on this equation in the limit of very large nonlinear dispersion $|c_2| \gg 1$, where the real part of the nonlinearity is neglected, show dispersive chaos [13]. Recently [14], it was found that for the range of values of c_1 and c_2 relevant to our experiment, the system exhibits bounded, chaotic solutions. These studies strongly suggest that it is the large value of the nonlinear dispersion coefficient, which dominates the dynamics.

In order to verify the relation between the collapse phenomena and the large nonlinear dispersion, we measured the value of c_2, as a function of ψ, by two methods. The first method uses the fact that the frequency of the TW

in a burst depends on the amplitude of convection. The change in the TW frequency, $\Delta\omega$, during the pulse evolution is given by $\Delta\omega = -gc_2/\tau_0|A|^2$. We use this relation in order to extract gc_2/τ_0. Then, the value of g is found by fitting the amplitude evolution of the pulse to Eq. (2). The value of c_2, shown as circles in Fig. 3, is obtained by averaging over many pulses. The second method, which was already used in Ref. [8], is based on the dependence of ω, on ϵ which follows from Eq. (2). By substituting the ansatz solution $A \sim \exp[i\omega(k)t + ikx]$ into Eq. (2), one finds (neglecting the spatial derivatives), $\tau_0 \frac{\partial\omega}{\partial\epsilon} = c_2$. Then, the value of c_2 was obtained from the dependence of the frequency of the localized TW state on ϵ. The results at different values of ψ, are shown as squares in Fig. 3. The values of c_2 obtained by the two methods are consistent, although the results of c_2 obtained by the second method at smaller values of $|\psi|$, are more negative (by about 30%). In accordance with previously measured [8,16], and calculated [6,7] results, the value of the nonlinear dispersion coefficient becomes more negative as $|\psi|$ decreases. Thus, for longer cells, at higher values of ϵ and smaller values of $|\psi|$, the dynamics of the "blinking" state become dominated by the nonlinear dispersion. Figure 2(c) shows the temporal behavior of the amplitude in our numerical simulations, which is qualitatively similar to that of Fig. 2(a).

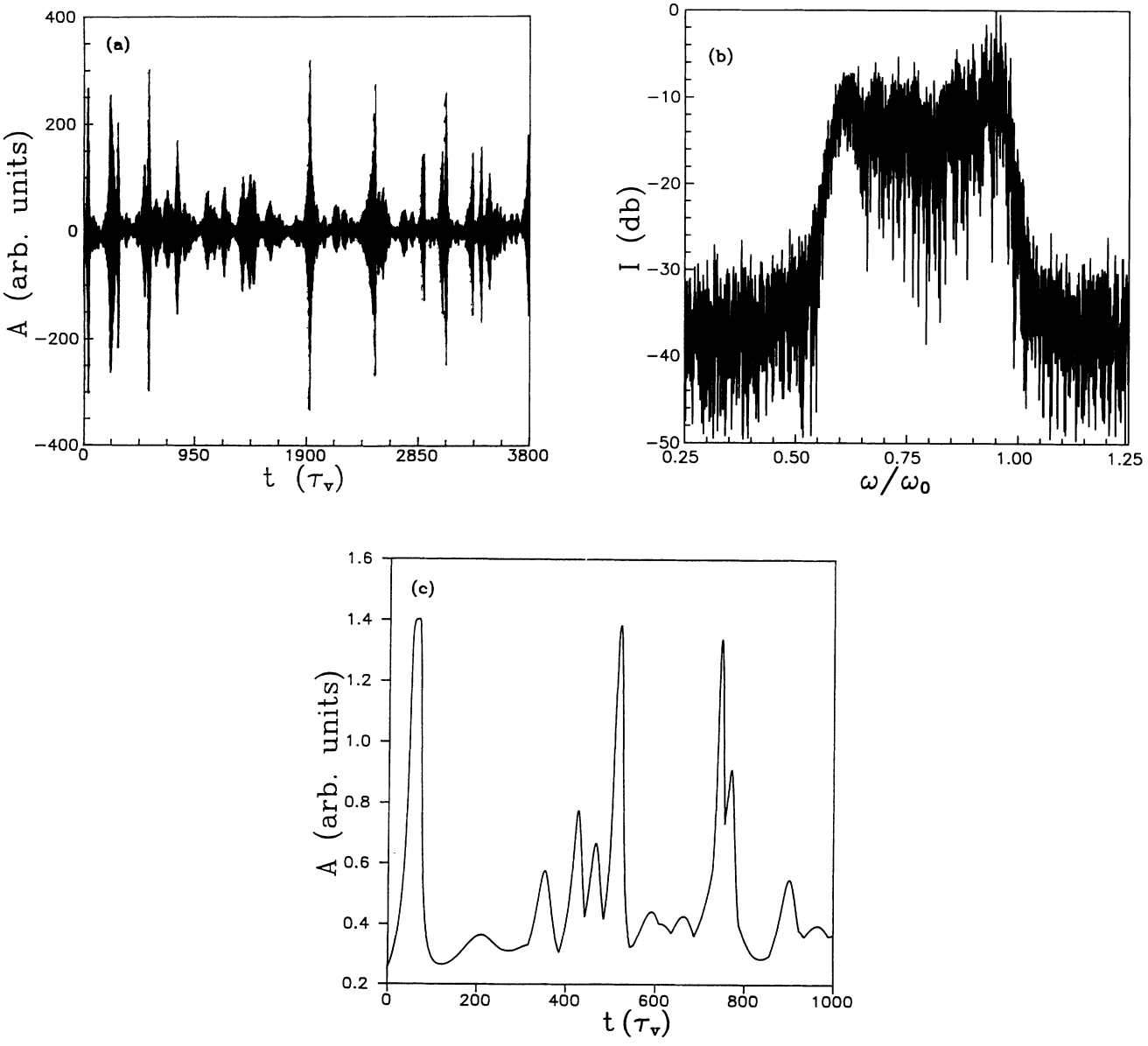

FIG. 2. (a) Temporal dependence of the intensity of the shadowgraph signal for the same values of parameters as in Fig. 1. (b) Power spectrum of the data shown in (a). ω_0 is the critical TW frequency. (c) Temporal dependence at one spatial point, obtained from numerical integration of the 1D CGL equation. $\epsilon = 0.01, c_2 = -7$. Note the qualitative similarity to (a).

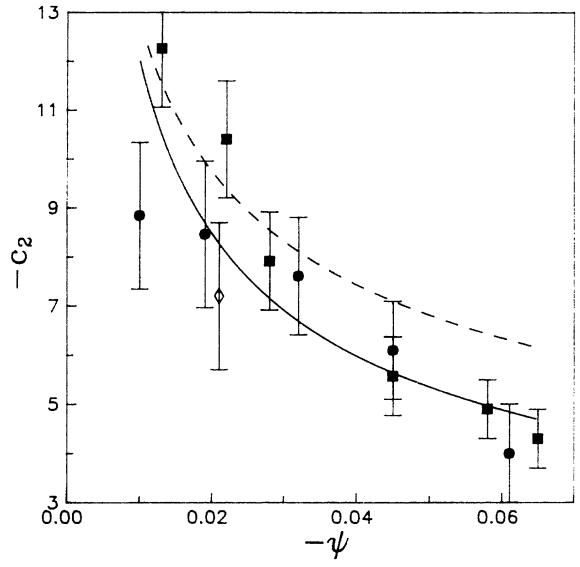

FIG. 3. The value of the nonlinear dispersion coefficient c_2 as a function of ψ. Circles: values of c_2 obtained from the dependence of the frequency on the amplitude of the pulses. Squares: values of c_2 obtained from the dependence of the frequency on ϵ in the localized TW state. The diamond point is taken from Ref. [13]. The dotted line is a power law fit to the theoretically computed values of c_2 [7]. The full line is a power law fit to the experimental data. The experimental fit parameters deviate from the theoretical parameters by $\sim 15\%$.

The complicated temporal behavior described above suggests that the phase of the convection amplitude should rapidly lose coherence. Thus we checked the cross correlation of the phase field $|G|(\Delta x, \Delta t) = |\langle \phi(x,t)\phi(\Delta x + x, \Delta t + t)\rangle|$, where ϕ is the local phase of the measured amplitude $A = a \exp i\phi$. Unexpectedly, in addition to an algebraic decay near $\Delta x = 0, \Delta t = 0$, we found that the cross-correlation function was not decaying to zero for large decay times, Δt. In fact, small amplitude irregular behavior (which is definitely above the noise level) was observed, even for very large values of Δt. Figure 4(a) clearly points out on this behavior. We suggest, that this behavior can be related to radiation of small amplitude waves during the burst collapse, and their absorption during bursting. We consider the bursts as the coherent structure: thus, the small amplitude field that is radiated at the collapse should be coherent with the burst, generating the tail of G. In Fig. 4(b) we show results of the absolute value of the cross-correlation function computed from numerical simulations of the 1D-CGL equation. The similarity with the experimental results is obvious. The oscillations of the the cross-correlation function indicate the existence of some long time scale in the system, which remains to be explained. It is not, however, related to the round trip time of the traveling waves. We could not find any significant dependence of the algebraic exponent coefficient on ϵ.

Let us now concentrate on the spatiotemporal evolution of a single burst. Figure 5 presents the temporal evolution of the amplitude and width of such a single pulse (the width is defined at FWHM of the pulse, and is measured in units of the cell height d). The solid lines in Fig. 5 are results of numerical simulations, performed at $\epsilon = 0.004$, $\xi_0^2 = 0.148$, $\tau_0 = 0.1$, $c_1 = 0$, $g = 0.2$, and $c_2 = -9$. One can divide the pulse evolution into three stages: linear exponential amplitude growth, followed by a faster than exponential growth due to the nonstabilizing effect of the nonlinear term in Eq. (2), and finally, the collapse. During the linear growth, the pulse amplitude increases exponentially, and the pulse becomes slightly wider. During the nonlinear stage, the amplitude growth is followed by accelerated narrowing of the

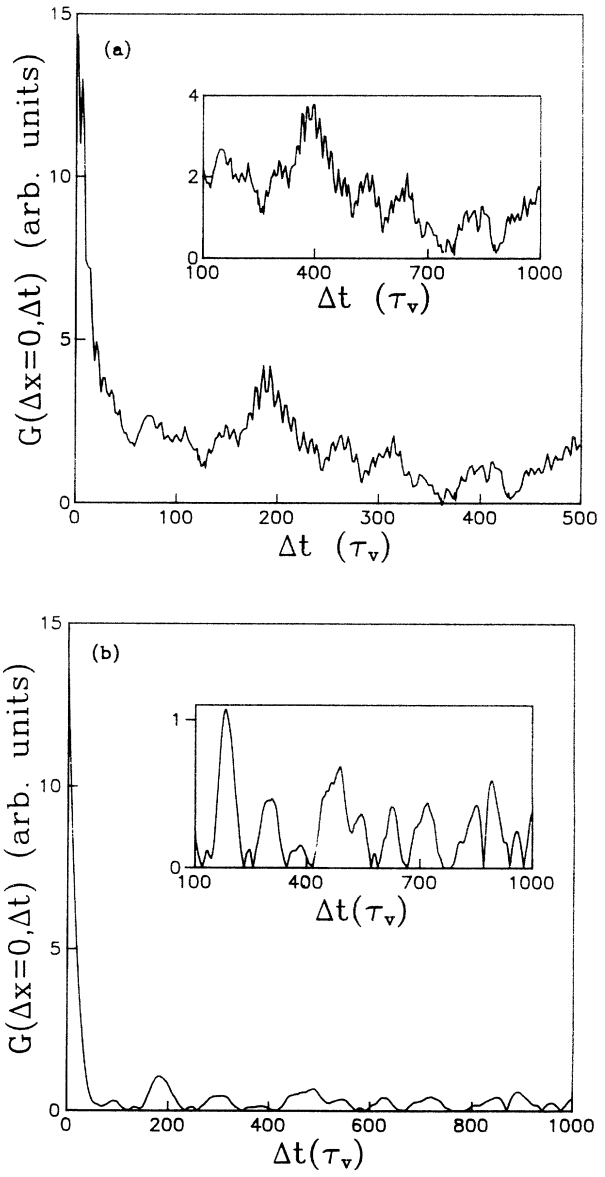

FIG. 4. (a) Envelope of the phase autocorrelation function of the optical signal $|G|(\Delta t)$. $\psi = -0.019; \epsilon = 0.007$; $c_2 = -8.8; \Gamma = 40.6$. (b) Envelope of the phase autocorrelation function obtained by numerical simulations of CGL equation at $\epsilon = 0.01, c_2 = -10$. The insets show the details for the small amplitudes at longer delays.

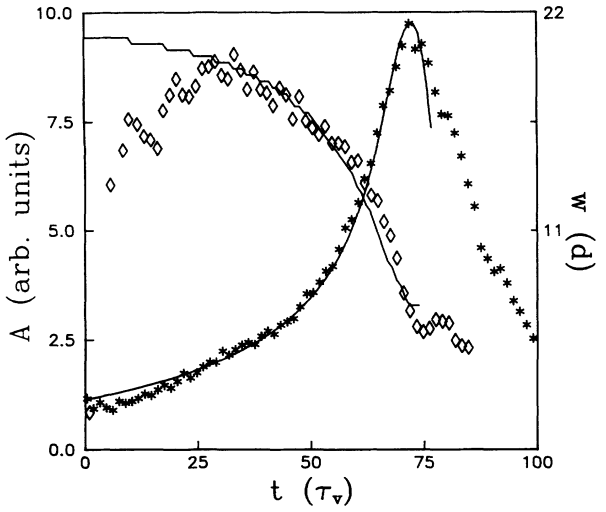

FIG. 5. Temporal evolution of the maximal amplitude of a single burst (circles) and its width (squares). Solid lines are the results of numerical simulations. (ψ=-0.019; ϵ=0.004; Γ=40.6).

pulse to a width of $O(d)$. The collapse is initiated as a result of the compression of the pulse at the edges. As the pulse evolves, a wave number gradient builds up in the vicinity of the pulse's maximal amplitude [Fig. 6(a)]. This gradient becomes steeper as evolution proceeds, and finally, relaxes as collapse occurs. Figure 6(b) shows the same effect obtained by numerical simulations. Note that the experimental values of the wave number gradients are slightly larger than the numerically obtained ones. The asymmetry in the wave number deviations disappear as the pulse narrows and separates from the lateral wall.

When the pulse becomes narrow enough, its amplitude decays rapidly to a very small value. We denote the moment at which the decay begins as $t = t_c$. The experimental decay is slightly slower than the numerical one.

This self-focusing scenario seems to have a threshold: the faster than exponential growth and collapse are observed only if the initial pulse is sufficiently wide. As is shown in Fig. 7(a), a narrow pulse grows only exponentially. In fact, as we shall explain in detail in the next section, the evolution of narrow pulses is explained by the mechanism suggested by Bretherton and Spiegel [13]. Figure 8(a) shows the dependence of the ratio between the maximal amplitude of the burst to its initial amplitude, $\frac{A_f}{A_i}$, on the initial pulse width w. A transition between the two evolution mechanisms near $w = 10$ is evident. Figures 8(b) and 8(c) provide another, numerical confirmation of this point. In Fig. 8(c), one can see that for initially narrow pulses the maximal amplitude reached by the pulse before its collapse relates linearly to the initial pulse amplitude. This dependence becomes stronger as the pulse width increases.

At the beginning of this section we suggested that in our experiments, one can neglect the effects of nonlinear interaction, nonlinear saturation, and reflection, and use Eq. (2) as the model equation. The close matching between the experimental and the numerical results strongly supports the applicability of this model.

While the temporal growth is strongly nonsymmetric, the high amplitude parts of the spatial profile of a burst is symmetric and self-similar during most of the growth and decay processes. Figure 9(a) presents data of the spatial amplitude profile of the pulse at different stages of the evolution. The asymmetry in the small amplitude seen in Fig. 9(a) comes, probably from small inhomogeneities in the initial profile of the pulse. The latter induce [through Eq. (4), see below], small differences in the wave number profile, that affect the local growth

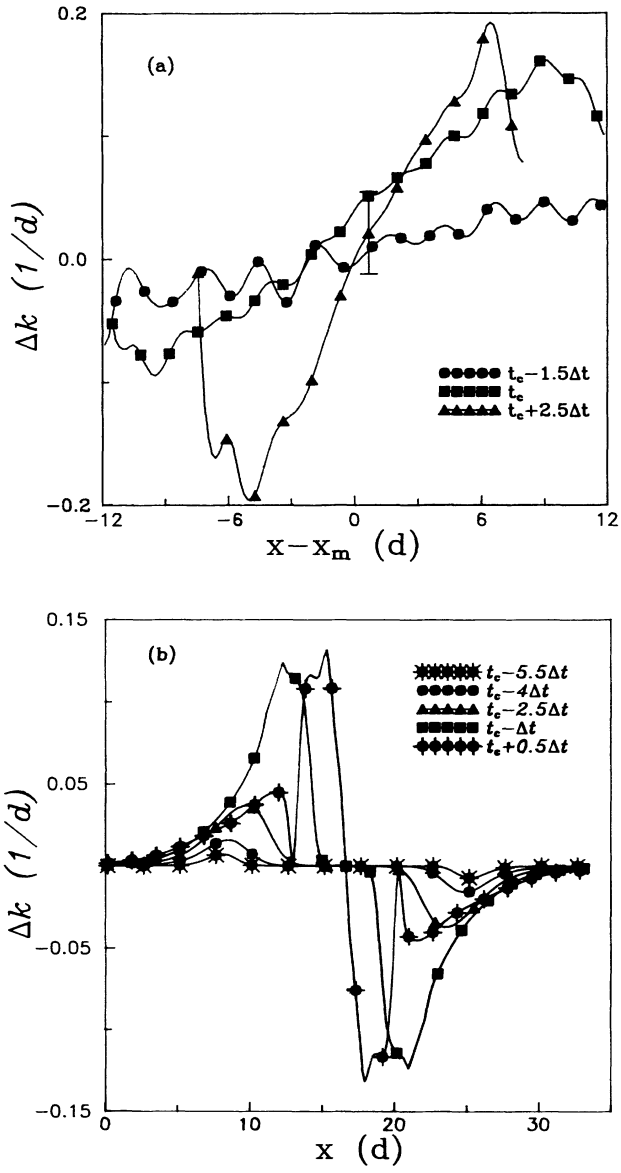

FIG. 6. The deviations from critical wave number, Δk, at different moments during the burst evolution and collapse. (a) Experimental data. The experimental parameters are the same as in Fig. 5. x_m is the position of the peak of the pulse. (b) Data obtained from numerical simulations of Eq. (2). The time step between profiles is $\Delta t = 10\tau_v$.

rate [Eq. (3)]. This effect, however, is less significant for the high amplitude parts, where nonlinearity becomes the dominant factor determining the pulse shape. Figure 9(b) shows a geometrically scaled version of the same profiles. As will be shown in the next section, the CGL equation predicts self-similar evolution for only a very limited part of the burst and collapse processes during

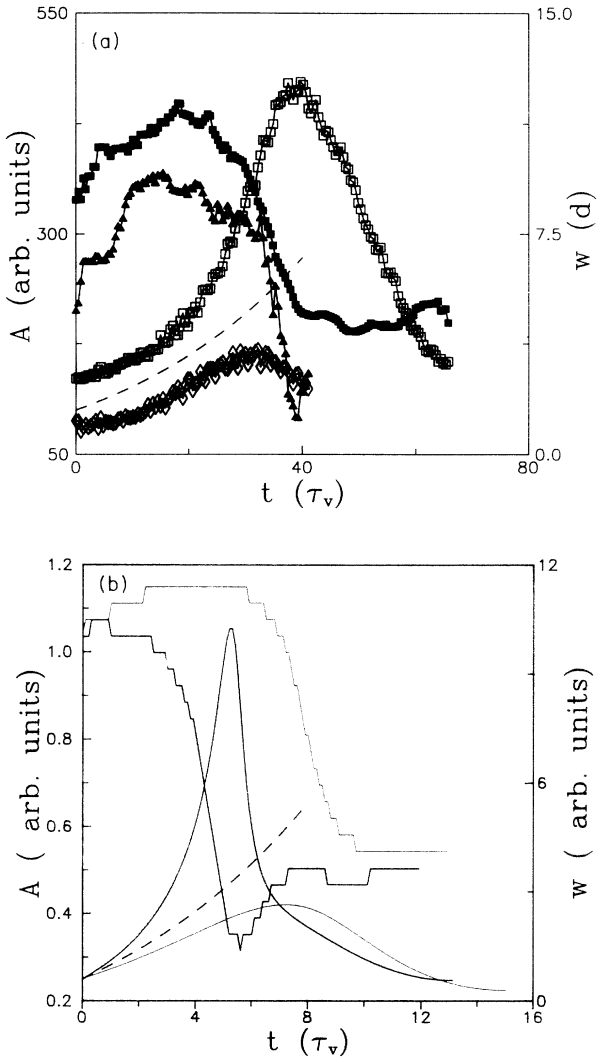

FIG. 7. (a) Comparison between pulse evolution of an initially narrow ($w \approx 9$) and an initially wide ($w \approx 11.5$) pulse. Square symbols stand for the wide pulse, and triangles for the narrow one. The empty symbols show amplitude evolution, and the full symbols present the pulse width. The amplitude of the wide pulse is shifted by 50 units in order to make the figure clearer. The dashed line described the linear growth $A = ae^{\epsilon t/\tau_0}$. Note that the width of the narrow pulse decreases significantly only after decay has begun, while the narrowing of the wide pulse is almost completed before collapse begins. $\epsilon = 0.009; \psi = -0.032; \Gamma = 43$. (b) Numerical comparison of the amplitude and the pulse width of burst and collapse behavior between the present mechanism (thick lines) and the mechanism of Bretherton and Spiegel, proposed in Ref. [13] (thin lines). $\epsilon = 0.012, c_2 = -7$. The dashed curve is the purely exponential growth $a_0 e^{\epsilon t/\tau_0}$.

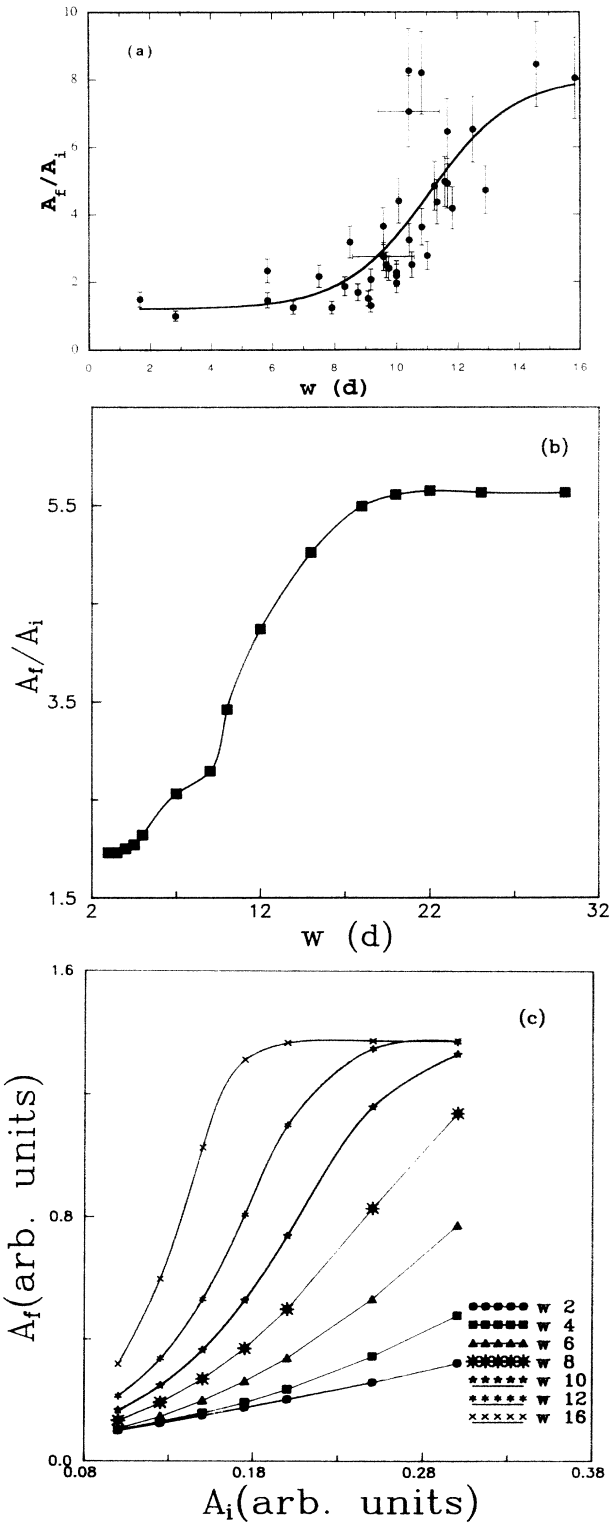

FIG. 8. (a) The ratio of the maximal amplitude reached by the bursts, A_f, to their initial amplitude, A_i as a function of the width of the bursts. A sharp transition near $w = 10$ is evident. $\psi = -0.032; \epsilon = 0.009; \Gamma = 40.6$. The solid line is a fit to a $y = c + \tanh^{-1}(\frac{x-x_0}{b})$. (b) The same as in (a), for data obtained from numerical simulations of the CGL equation at $\epsilon = 0.01, c_2 = -10$. (c) The dependence of A_f on the initial amplitude A_i for several values of initial width w as obtained numerically.

which the relation $A \sim w^{-1}$ holds. While such dependence was found in part of the pulse evolution (see next section), it is remarkable that self-similar evolution (although only in the geometrical sense, i.e., by normalizing separately the height and the width of the profiles) was actually observed for much longer part of the process.

At higher values of ϵ, where the transition to the LTW state is approached, the character of the "blinking" state changes, as can be seen from Fig. 10. Instead of the sharp bursting and collapse described above, one observes rather often a sequence of two pulses, which decay slowly. We believe that the appearance of such "double hump" pulses has to do with a new mechanism (such as the redistribution of the concentration [23] that becomes important near the transition to the LTW state. Our model cannot account for this behavior.

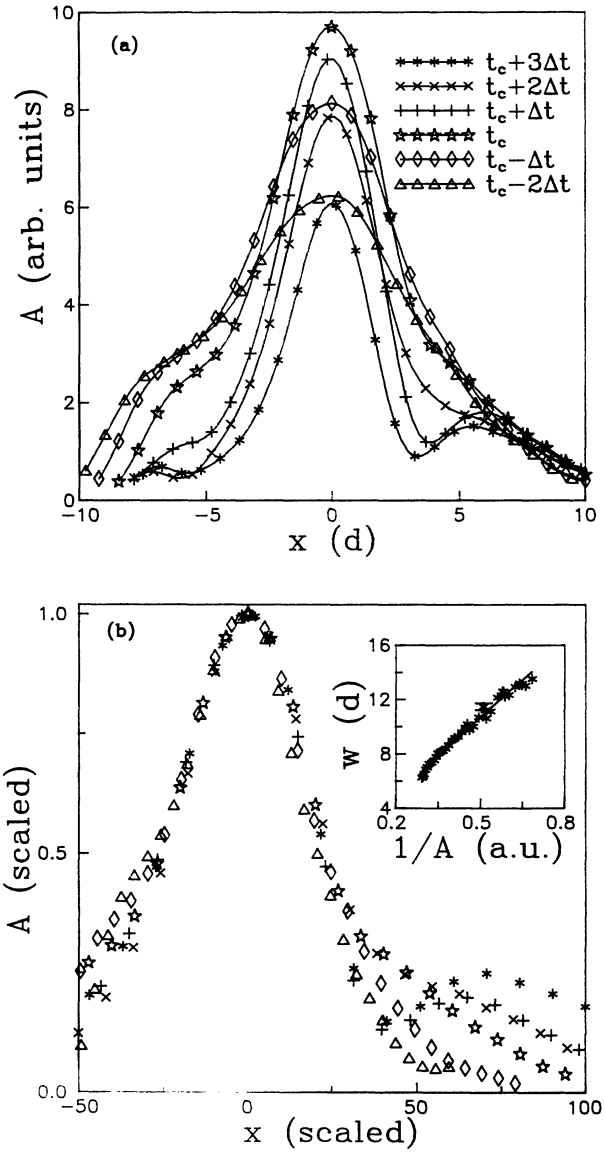

FIG. 9. (a) Spatiotemporal evolution of a single burst. Time step between profiles $\Delta t = 5\tau_v$. (b) Scaled profiles of (a). The inset: relation between the pulse amplitude and width during evolution. The solid line has a -1 slope. The scaling was obtained by normalizing the height and width of each profile to 1 and 50, respectively. The experimental parameters are identical to those stated in Fig. 5.

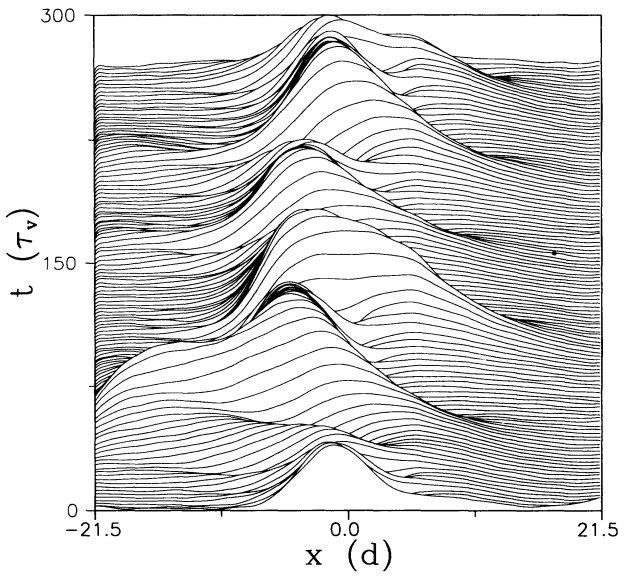

FIG. 10. Hidden line presentation of the spatiotemporal dynamics of the convection near the transition to the LTW state. $\epsilon = 0.012; \psi = -0.019; \Gamma = 43$. The transition to the LTW state occurs at $\epsilon = 0.0134$.

IV. THEORETICAL ANALYSIS

In Refs. [15] and [16], the authors suggested that the erratic behavior described above occurs due to the large value of the nonlinear dispersion coefficient c_2 in Eq. (2). The suggestion was based on the similarity between experimental results and numerical simulations performed in the limit of strong nonlinear dispersion [13,14]. The similarity remained, however, mainly qualitative. We would like to present a coherent picture here, based on the CGL equation, that can explain most of the experimental and numerical results described above. We begin our analysis with Eq. (2), where we notice that g is positive, $|c_1| \ll 1$ [5] and $|c_2| \gg 1$ [6]. Thus, we may neglect the linear dispersion coefficient c_1. We cannot, however, neglect the real part of the coefficient of the nonlinear term, since it is crucial for the understanding of the faster than exponential growth shown in Fig. 5. We rewrite Eq. (2) in a frame moving with velocity s, in terms of the phase and the amplitude $A = a \exp(i\phi)$:

$$\tau_0 \partial_t a = (\epsilon - \xi_0^2 k^2) a + \xi_0^2 \partial_x^2 a + g a^3, \tag{3}$$

$$\tau_0 \partial_t k = \xi_0^2 \partial_x (a^{-2} \partial_x (a^2 k)) + g c_2 \partial_x a^2, \tag{4}$$

where $k = \phi_x$ is the local deviation from the critical wave number. As can be seen from Fig. 5, at the beginning of the nonlinear evolution, a wide, small amplitude hump is formed. At this stage $k \ll \sqrt{\frac{\epsilon}{\xi_0^2}} \sim 0.1$, i.e., dissipation

does not play an important role. We also assume that far from its edges, the burst is uniform, i.e., a_{xx} is small. In this case, Eq. (3) can be solved explicitly to yield the faster than exponential evolution:

$$a^2 = \frac{\epsilon}{g}\{\exp[2\epsilon/\tau_0(t^* - t)] - 1\}^{-1}. \quad (5)$$

Here, a singularity is reached at a finite time $t \to t^*$. For times close to t^*, the solution reduces to $a^2 \sim (t^* - t)^{-1}$, where t^* is the theoretical collapse time. However, a real singularity cannot be reached, since the description by the CGL equation loses validity at sufficiently large amplitude. Nevertheless, we found that the maximal amplitude of the pulse could be described by Eq. (5), almost up to the experimental collapse, which starts at $t = t_c$. From Fig. 6(b), we can see that until very close to t_c, the wave number distribution at the peak is flat. Collapse occurs only when the width of this plateau becomes close to the roll size. We found that $t^* - t_c$ is $\sim 10\tau_0$, i.e., the pulses approach the singularity rather closely. Thus, we conclude that dissipation effects become important only very close to the collapse moment.

In order to further compare the experimental results with the theoretically derived solution, let us check the statistical characteristics of the burst evolution. We now introduce the probability distribution function (PDF) [2]:

$$P(|h|) = \frac{\int dtdx\delta(|h| - |a(x,t)|)}{\int dtdx}. \quad (6)$$

By substituting the solution given by Eq. (5) and integrating over the pulse evolution time, we get

$$P(|h|) \sim \frac{1}{|h|(\epsilon + 2g|h|^2)}. \quad (7)$$

Figure 11 presents experimental PDF data. One can clearly distinguish three regimes in the data. The linear regime, having a slope of (-1) corresponds to the early evolution of the pulse. The nonlinear evolution stage, showing a slope of (-3) , and the approach to collapse, showing much steeper dependence on the amplitude due to the renormalization of ϵ by $\xi_0^2 k^2$. Thus, we are able to explain most features of the burst evolution in the framework of the CGL equation.

The central question of the bursting process concerns the behind the pulse collapse. From Eq. (4) one can easily see that wave number deviations are induced by amplitude gradients. At early evolution, the pulse profile is wide and essentially flat. Thus, the largest amplitude gradients occur near the pulse edges, which act as a source of large k. At the edges, the pulse growth is suppressed by $\xi_0^2 k^2$, while at the core of the pulse the amplitude continues to grow more rapidly than an exponential, following Eq. (5). This process causes self focusing of the pulse (see Fig. 5) which rapidly becomes higher and narrower. Eventually, collapse occurs due to compression. It is only when the wave number deviations become sufficiently large (as the pulse width reduces to $\sim 1d$), that the effective growth rate $(\epsilon + ga^2 - \xi_0^2 k^2)$ becomes negative, and collapse takes place. The value of k

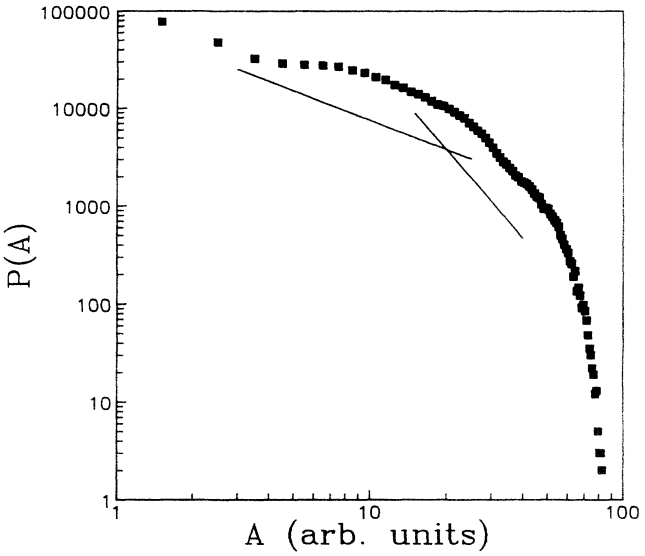

FIG. 11. PDF of the amplitude during the burst evolution. The data shows gradual transition from $P \sim A^{-1}$ (the solid line has a slope of -1), to $P \sim A^{-3}$ (the dotted line), and a sharp decay due to to dissipation at high amplitudes. $\psi = -0.022, \epsilon = 0.008, \Gamma = 34.7$.

continues to grow even after collapse has begun [see the second term on the right hand side of Eq. (5)], accelerating the amplitude decay to very small values. Figure 6 shows the development of k profiles during the burst evolution and collapse.

Let us now look more carefully on the differences between the Bretherton-Spiegel [13], and the mechanism suggested by us. The presence of the nonlinear term ga^3 in Eq. (3), which is neglected in the numerical treatment of Ref. [13], is of the most crucial importance for understanding the high amplitude bursting behavior, and leads to entirely different dynamics, coined by us "self focusing." Figure 7(b) compares the results of numerical integration of the CGL with (thick lines) and without (thin lines) this term. Upon neglecting ga^3, Eq. (3) becomes linear, and the pulse evolution is slower than exponential. The decay is generated due to the renormalization of ϵ by the wave number deviations, and the width of the pulse remains almost constant until a moment which is very close to the beginning of the amplitude decay.

The mechanism suggested by us is nonlinear and shows clear self-focusing behavior. The growth is faster than exponential, and destruction occurs through compression of the pulse from the sides, as explained above. Thus, narrowing begins as the amplitude increases, and is accelerated as the amplitude evolves, through Eq. (4). Due to the nonlinear term in Eq. (3), the amplitude continues to grow even after the renormalized growth rate $(\epsilon - \xi_0^2 k^2)$, becomes negative. Figure 7(b) clearly demonstrates the sharper and narrower profile of the pulses evolved according to Eq. (3) relative to the behavior observed while neglecting the nonlinear term of this equation. The fact that the burst evolution is a threshold phenomenon [Figs. 8(a), 8(b), and 8(c)], strongly supports the distinction

suggested above: for initially narrow pulses wave number deviations affect the center of the pulse almost immediately after evolution begins, thereby activating the ϵ renormalization mechanism suggested by Bretherton and Spiegel [13] and used by Kolodner *et al.* [15,16], and destroying the pulse before it could grow significantly. Note that, when considering the nonlinear mechanism, the large value of the nonlinear dispersion coefficient c_2 is crucial solely to the collapse process, while it is the real part of the nonlinear coefficient which affects the growth of the pulse and its self-focusing behavior.

A numerical analysis of burst and collapse occurring in the quintic CGL equation was recently considered [2]. In this paper, singular solutions of the 1D-CGL equation with quintic nonlinearity were studied in the inviscid limit. In this limit, the CGL equation reduces to the NLS equation which has a singular solution blowing up in a finite time. In this model, growth and collapse are shown to be self-similar. This is true for the third order CGL as well. When the pulse amplitude is strongly nonlinear, the linear term ϵA in the CGL equation is small with respect to the nonlinear term, and the CGL equation becomes the NLS equation:

$$\tau_0 A_t = \xi_0^2 A_{xx} + g(1 + ic_2)|A|^2 A. \tag{8}$$

In this limit, the CGL equation has the following symmetry: if $A(x,t)$ is a solution, so is $\lambda A(\lambda x, \lambda^2 t)$. Thus, the pulse is expected to grow self-similarly, with its height inversely proportional to its width. Note that this relation should be valid for only a small part of the pulse evolution. At early evolution the linear part cannot be neglected with respect to the nonlinear part. On the other hand, for too large amplitudes the CGL equation loses validity. Thus, it is remarkable that the pulse evolution shown in Fig. 8, is found to be self-similar at almost all stages. The self-similarity continues even at the decay stage, although the scaling changes. The inset in Fig. 8(b) shows the scaling of the burst width with its amplitude during most of the evolution. As expected, the slope is close to -1. Figure 12 shows scaled profiles of a pulse at different moments of its evolution and collapse, as obtained from numerical simulations. Self-similarity during evolution and collapse is evident.

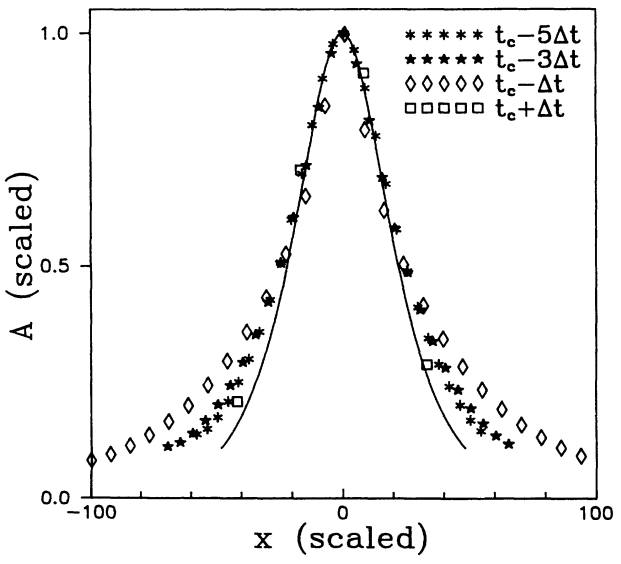

FIG. 12. Numerical simulations of spatiotemporal evolution of a single pulse presented in scaled variables. The time step between profiles is $\Delta t = 5\tau_v$. The solid line is a singular solution of the NLS equation.

V. CONCLUSIONS

In this paper, we presented experimental results on one-dimensional TW convection of a binary fluid in rectangular geometry, which is characterized by repetitive, chaotic bursting and collapse of the wave amplitude. In rectangular geometry, left- and right-going TW are usually present, and their interaction, as well as reflection at the endwalls, are important to the dynamics in short convection cells and at large values of the separation ratio $|\psi|$, where the nonlinear dispersion is weaker [3]. This behavior manifests itself in the regularly modulated "blinking" state, and was observed experimentally in cells of small aspect ratio $\Gamma = 10, 12$ [3], for specially tuned values of the aspect ratio [21], and also in the numerical simulations performed by Cross, where dispersion was not taken into account at all [11].

The situation changes dramatically as the experimental parameters are changed. By reducing the value of $|\psi|$ one can increase the nonlinear dispersion of the system. Increasing ϵ accelerates the growth, causing nonlinearity to become important sooner. Finally, the role of reflection from the lateral sidewalls, as well as the role of nonlinear interaction between the left- and right-going TW become less important as the convection cell becomes longer. Thus, even at moderate aspect ratio $\Gamma = 20$, a transition between regularly modulated and chaotic blinking TW was observed [3]. In this paper, we presented results obtained in very long cells ($\Gamma = 34.7, 40.6$), in which only chaotic behavior was observed. The fact that the interaction between the left- and the right-going TW is negligible enabled us to analyze the results in the framework of a single CGL equation. It is interesting to note, however, that in a recent numerical study [22], we found that even in the case that the nonlinear interactions are included in the model, the dynamics do not change qualitatively.

Analysis of the CGL equation suggests that bursting occurs due to the destabilizing role of the real part of the nonlinear term in the equation, which leads to the formation of a singularity in a finite time. This singularity cannot be actually reached, though, due to the strong nonlinear dispersion of the system, which, through phase winding causes compression of the pulse and its collapse. Thus, one has to consider both the real and the imaginary parts of the cubic nonlinear term in the CGL equation, in order to fully account for the observed behavior. Our experimental results, as well as the numerical simulations performed by us, show that a single 1D-CGL equation can quantitatively describe all the main features of the state.

The spatiotemporal behavior observed in our experiments is very similar, at least qualitatively, to the observations presented in Refs. [15] and [16]. In annular cells, endwall reflection does not exist. Also, in this geometry a state of unidirectional TW can be prepared. Thus, the use of Eq. (2) can be rigorously justified [16,15]. While the dynamics observed in an annular geometry is probably more spectacular, it is essentially identical to the dynamics observed in long rectangular cells for similar parameters.

The mechanism suggested above reduces, for initially narrow pulses ($w < 10d$), to the linear mechanism of Ref. 13. At higher values of ϵ, close to the transition to the LTW state, our mechanism breaks down, and "double hump" bursts, showing much slower amplitude decay appear. Thus, the validity of our mechanism is limited by the Bretherton-Spiegel mechanism from one side, and by the nonvariational effects that lead to the appearance of the LTW state, on the other.

A few questions remain open. At the beginning of the evolution, a wide "hump" is formed. What is the mechanism responsible for the creation of this hump remains to be understood. We cannot provide a satisfactory quantitative explanation as to the long time behavior of the phase cross-correlation function $|G|$. The fact that the amplitude of $|G|$ stays well above the noise level even for long time delays, as well as its seemingly periodic behavior, which we could not connect to any experimental time scale, remains a puzzle to us.

In conclusion, our experiments revealed a pulse self-focusing and collapse mechanism that originates in the large nonlinear dispersion of the system and the large phase gradients at the edges of the pulse.

ACKNOWLEDGMENTS

We acknowledge fruitful discussions with L. Kramer, G. Fal'kovich, and P. Kolodner. This work was partially supported by the US-Israeli BSF Grant No. 90-00412. The Israel Science Foundation grant, The Landau-Weizmann program, the Russian Foundation of Fundamental Studies, and the German-Israel Foundation (GIF) Grant No. I-130091.

[1] V. E. Zakharov, in *Handbook of Plasma Physics*, edited by A. Galeev and R. Sudan (Elsevier, New York, 1984), Vol. 3.
[2] H. Iwasaki and S. Toh, Prog. Theor. Phys. **87**, 1127 (1992).
[3] J. Fineberg, E. Moses, and V. Steinberg, Phys. Rev. Lett. **61**, 838 (1988); V. Steinberg, J. Fineberg, E. Moses, and I. Rehberg, Physica D **37**, 359 (1989).
[4] P. Kolodner and C. M. Surko, Phys. Rev. Lett. **61**, 842 (1988); P. Kolodner, C. M. Surko, and H. Williams, Physica D **37**, 319 (1989).
[5] M. C. Cross and K. Kim. Phys. Rev. A **37**, 3909 (1988).
[6] W. Schopf and W. Zimmermann, Europhys. Lett. **8**, 41 (1989).
[7] W. Schopf and W. Zimmermann, Phys. Rev. E **47**, 1739 (1993).
[8] V. Steinberg and E. Kaplan, in *Spontaneous Formation of Space-Time Structures and Criticallity*, edited by T. Riste and D. Sherrington (Kluwer, Boston, 1991), pp. 207–244.
[9] M. S. Bourzutschky and M. C. Cross, Phys. Rev, A **45** 45,8317 (1992).
[10] E. Kaplan and V. Steinberg, Phys. Rev. E **48**, 661 (1993).
[11] M. C. Cross, Phys Rev. Lett. **57**, 2935 (1986); M. C. Cross, Phys. Rev. A **38**, 3593 (1988).
[12] P. Coullet, S. Fauve, and E. Tirapegui, J. Phys. Lett. **46**, L-787 (1985); E. Knobloch, Phys. Rev. A **34**, 1538 (1986).
[13] C. S. Bretherton and E. A. Spiegel, Phys. Lett. **96A**, 152 (1983).
[14] W. Schopf and L. Kramer, Phys. Rev. Lett. **66**, 2316 (1991).
[15] P. Kolodner, J. Glazier, and H. Williams, Phys. Lett. Rev. **65**, 1579 (1990).
[16] J. Glazier, P. Kolodner, and H. Williams, J. Stat. Phys **64**, 945 (1991).
[17] E. Kaplan and V. Steinberg, Europhys. Lett. (to be published).
[18] S. Rasenat *et al.*, Exp. Fluids **7**, 412 (1989).
[19] P. Y. Ktonas and N. Papp, Signal Processing **2**, 373 (1980).
[20] J. Fineberg, V. Steinberg, and P. Kolodner, Phys. Rev. A **41**, 5743 (1990).
[21] P. Kolodner, Phys. Rev. E **47**, 1038 (1993).
[22] E. Kaplan, Ph.D. thesis, The Weizmann Institute of Science (1994).
[23] P. Kolodner (private communication).